Original Article

Optimization of a Brayton external combustion gas-turbine system for extended range electric vehicles

Wissam S Bou Nader[1,3], Charbel J Mansour[2] and Maroun G Nemer[1]

[1] Ecole des Mines de Paris, Center for Energy Efficiency of Systems, Palaiseau, France
[2] Lebanese American University, Industrial and Mechanical Engineering Department, New York, United-States
[3] PSA Group, Centre technique de Vélizy, Vélizy, France

Abstract

Significant research efforts are considered in the automotive industry on the use of low-carbon fuels in order to reduce the emissions and improve the fuel economy of vehicles. Some of these fuels, such as the solid fuels for example, are only compatible with external combustion machines. These machines are only suitable for electrified powertrains relying on electric propulsion, in particular the extended-range-electric-vehicles with series hybrid powertrain configuration where fuel consumption strongly relies on the energy converter efficiency and power density. This paper investigates the fuel savings potential of these vehicles using a Brayton external combustion gas-turbine system as energy converter substitute to the conventional internal combustion engine. An exergo-technological explicit analysis is conducted to identify the best system configuration. A downstream-intercooled reheat external combustion gas-turbine (DIRe-ECGT) system is prioritized, offering the highest efficiency among the investigated systems. An extended-range-electric-vehicle model is developed and energy consumption simulations are performed on the worldwide-harmonized light vehicles test cycle. Fuel consumption simulation results are compared to a reference extended-range-electric-vehicle using an engine auxiliary-power-unit. Results show 6% to 11.5% of fuel savings with the prioritized DIRe-ECGT auxiliary-power-unit as compared to the reference model, depending on the battery capacity and the trip distance.

Keywords

External combustion gas-turbine, Brayton cycle, exergy analysis, extended-range-electric-vehicle, series hybrid, dynamic programming.

Nomenclature

AC	Alternative Current
APU	Auxiliary Power Unit
CC	Combustion Chamber
CCB	Combustion Chamber Blower
DC	Direct Current
DP	Dynamic Programming
ECGT	External Combustion Gas Turbine
EMS	Energy Management Startegy
EREV	Extended Range Electric Vehicle
GHG	Greenhouse Gas
GT	Gas Turbine
HEX	Heat Exchanger
ICE	Internal Combustion Engine
NSGA	Non-dominated Sorting Genetic Algorithm
SOC	State Of Charge
WLTC	Worldwide-harmonized Light vehicles Test Cycle
S-ECGT	Simple ECGT
R-ECGT-1	Regenerative ECGT – configuration 1
R-ECGT-2	Regenerative ECGT – configuration 2
DS-ECGT	Downstream simple ECGT

I-ECGT Intercooled ECGT
IR-ECGT-1 Intercooled regenerative ECGT – configuration 1
IR-ECGT-2 Intercooled regenerative ECGT – configuration 2
DI-ECGT Downstream intercooled ECGT
IRe-ECGT Intercooled reheat ECGT
IRRe-ECGT-1 Intercooled regenerative reheat ECGT – configuration 1
IRReECGT-2 Intercooled regenerative reheat ECGT – configuration 2
DIRe-ECGT Downstream intercooled reheat ECGT
DIcRe-ECGT Downstream isothermal compression reheat ECGT
DIcIe-ECGT Downstream isothermal compression isothermal expansion ECGT

1. Introduction

Automotive manufacturers are investigating the use of alternative fuels in order to comply with GHG and pollutant emissions regulations. Some alternative fuels are compatible with internal combustion engines [1], however others such as solid fuels require the use of external combustion machines, adapted for automotive applications. Many of these machines, namely the external combustion gas turbine (ECGT) [2, 3], Rankine machines [4], Stirling engines [5, 6], Ericsson engines [7], thermoacoustic [8] and thermoelectric generators [9], have been extensively explored for micro-cogeneration but very few for automotive applications [10, 11], and none for the ECGT up to the authors knowledge.

The ECGT, main focus of this study, is based on a gas turbine machine operating according to a modified Brayton thermodynamic cycle, where the air working fluid is heated in a heat exchanger as illustrated in Figures 1 and 6 (a). This system offers many advantages compared to conventional internal combustion engines (ICE), namely a reduced number of moving parts, vibration-free operation, low maintenance cost, high durability, the absence of water-cooling system [12] and the multi-fuel capability [13]. However, similar to all turbine-based machines, ECGT presents two main drawbacks preventing their use in conventional vehicles: (1) the high fuel consumption and (2) the acceleration lag. These drawbacks are mainly caused by operating the turbine at high speed even in idle conditions, in addition to mechanically coupling the turbine to the vehicle-driving load, which lead to a low efficiency operating range of the system. Moreover, the use of a heat exchanger (HEX) in the ECGT adds a thermal inertia on the upstream of the turbine, which further worsens the acceleration lag, and makes the ECGT system non-compatible for fast response power delivery to follow the variable load applied in conventional powertrains.

Nonetheless, a review of recent research and development programs revealed interests in ECGT for a specific application, where the machine operates steadily at constant speed and drives an electric generator. Traverso et al [14] presented a significant reduction of fuel consumption while operating the ECGT at optimal efficiency point. Roquette et al [15] showed that the ECGT's energy efficiency increases with the operating load, and Pierobon et al [16] showed that the optimal efficiency is not necessarily at full load, and that it is rather reached at partial load.

Therefore, based on the aforementioned findings, ECGT-systems present a forthcoming potential for improving fuel economy and emissions of passenger vehicles, with the benefit of multi fuel-use flexibility; particularly, in extended range electric vehicles with a series hybrid powertrain configuration (EREV). These powertrains combine a thermal and an electric powertrain in a series energy-flow arrangement [17]. The thermal powertrain in this study is constituted of an ECGT-system and an electric generator, and is referred to as the Auxiliary Power Unit (APU). It operates steadily at the optimum efficiency and mainly used to recharge the battery once depleted. The electric powertrain provides the necessary traction power to overcome the driving load, and it also serves to recover the braking energy. It is important to note that the APU operating speed is cinematically

decoupled from the vehicle velocity; therefore, the ECGT operation is controlled to meet its best efficiency. Figure 2 illustrates the powertrain configuration of the modeled EREV and a simple ECGT-APU system.

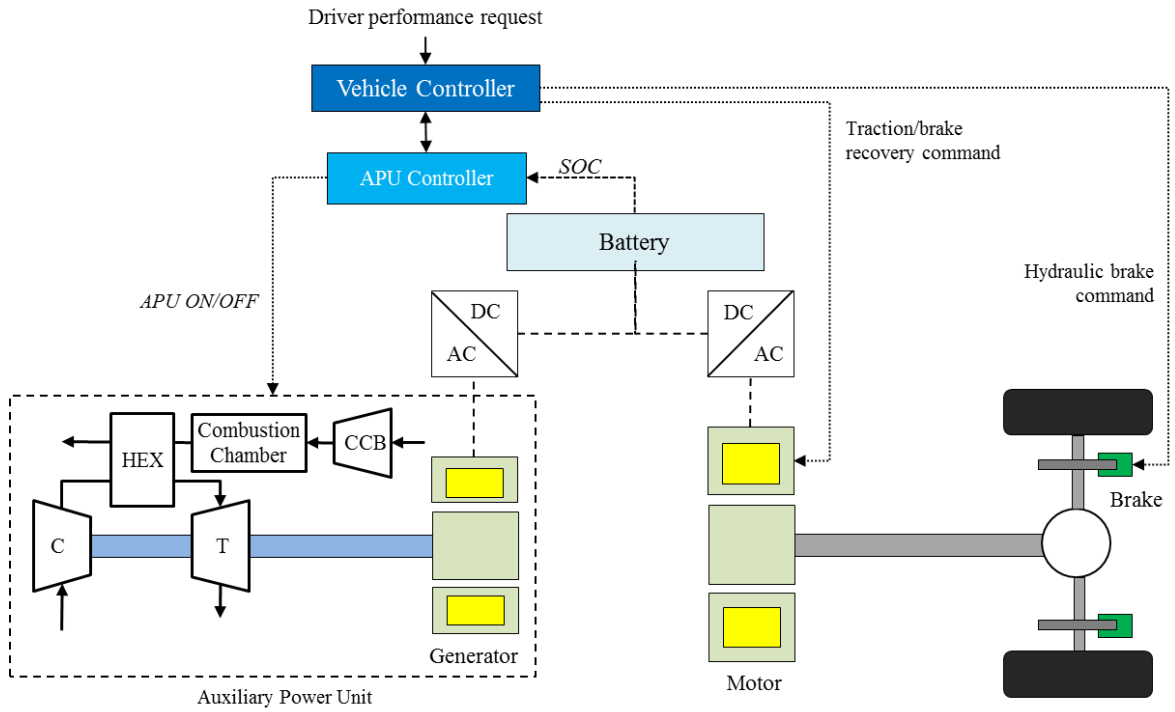

Figure 1: Configuration of the modelled EREV with a simple external combustion gas turbine APU.

On another hand, several ECGT-system options could be considered for integration in EREV, combining a simple ECGT to heat recovery systems and single or multiple-stage compressions and expansions. Few numbers of studies have been published over the past decade in the academic literature treating ECGT-system configurations and performance analysis [19, 20, 22]. The survey of these studies confirms that most ECGT-systems are designed based on efficiency optimization or on combined cycle overall optimum efficiency when coupled to bottoming cycle [15, 23]. However, there are no recent studies on ECGT-systems suitable for automotive applications, due to the lack of competitiveness of ECGT compared to ICE in conventional powertrains. Hence, the following main gaps and limitations in the recent literature are underlined:

- There are no studies assessing ECGT-systems performance based on a Brayton thermodynamic cycle for automotive applications.
- No specific methodology on selecting the best-suited ECGT-system for any type of application is adopted. The studies in the literature focus on the performance investigations of some ECGT-system configurations, without taking into consideration any optimization requirement or technological constraints.
- The overall vehicle consumption under driving conditions is not benchmarked against conventional vehicles and hybrid electric vehicles relying on internal combustion engines.

Therefore, based on the above synthesis of the insights and gaps in the literature for adopting ECGT in automotive applications, this study proposes a comprehensive methodology to identify the potential ECGT-system options and select the optimal system configuration for an EREV application. A methodology for the identification and assessment of the different ECGT-system options applicable to EREV is carried out in section 2, based on exergy analysis and automotive technological constraints. Observed results are then used for the prioritization and the selection of the optimal ECGT-system configuration. The selection criterion is optimizing the system efficiency. Thereafter,

the identified ECGT-system is integrated in an EREV model, developed in section 3, and a comparison between two EREV models with different APU technologies is presented: (1) an ECGT-APU and (2) a reference ICE-APU. Energy consumption simulations of these models are compared on the worldwide-harmonized light vehicles test cycle (WLTC), and a sensitivity analysis illustrating the battery size impact on energy consumption is presented. Note that Dynamic Programing (DP) is adopted as Energy Management Strategy (EMS) in order to provide the global optimal strategy to power ON and OFF the APU. Consequently, the analysis considers only the impact of the ECGT-system on consumption and excludes the influence of rule-based EMS [24, 25].

This study is novel in two ways: first, it is the first study to consider an exergo-technological explicit analysis for the prioritization and identification of the most efficient ECGT-system to be deployed in an EREV among a variety of possible ECGT-system options. Second, the study provides a comparative consumption assessment, between EREV of similar performance with ECGT-APU and ICE-APU.

2. Methodology for the Selection of Optimal External Combustion Gas Turbine System

This section presents the methodology adopted to evaluate the potential of ECGT-systems in an EREV with a series hybrid powertrain configuration. A similar methodology has been proposed by the authors in [17], for the selection of the optimal gas-turbine systems. The same approach, which consists of an exergy and a technological assessment, has been reconsidered in this study, and adapted to the case of ECGT, as summarized here below.

The methodology consists of two-steps assessment plan as illustrated in figure 2. The first assessment step consists of an energy and exergy analysis applied to the simple ECGT cycle, where the system efficiency, specific work, and exergy are calculated. Based on the resulting exergy destructions in the system, the simple ECGT is modified, and several system options are derived, while considering several measures to reduce exergy losses, such as heat recovery, reheat cycles and multi-stage compressions among others. Accordingly, the list of potential ECGT-system configurations is identified.

The energy and exergy calculations are then carried out in the second assessment step on all identified configurations. Components technological constraints and automotive design constraints are considered, and the optimal-realistic ECGT-system configuration for EREV application is selected.

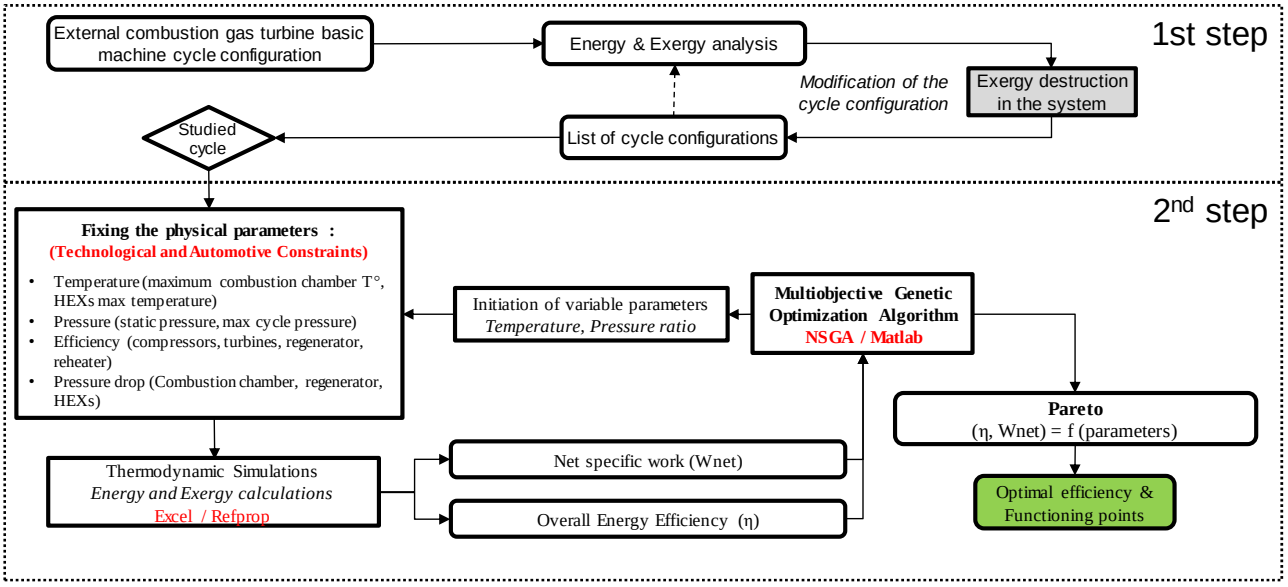

Fig. 2. Exergo-technological explicit selection method of the best-suited ECGT-system for EREV.

2.1. Energy and exergy analysis of simple external combustion gas-turbine system

This section presents the modeling of the simple ECGT-system. The system presents two loops: (1) a gas-turbine loop (GT) and a combustion chamber loop (CC), as illustrated in figures 1 and 6 (a). The GT-loop consists of a compressor, a heat exchanger and a turbine, whereas the CC-loop includes a combustion chamber blower (CCB) and a combustion chamber. Both loops exchange heat in the common HEX. It is important to note that air is considered as the working fluid in both loops for simplification.

First law of thermodynamics is applied to each component in order to deduce the cycle efficiency and power density.

The compressor, the CCB and the turbine steady-state work are determined using equations (1) to (3), by neglecting the heat exchange with the surroundings and the variation in potential and kinetic energy between inlet and outlet of the components.

$$w_{Compressor} = h_{C_{outlet}} - h_{C_{inlet}} \quad (1)$$

$$w_{CCB} = h_{CCB_{outlet}} - h_{CCB_{inlet}} \quad (2)$$

$$w_{Turbine} = h_{T_{outlet}} - h_{T_{inlet}} \quad (3)$$

With
$w_{Compressor}$: Compressor specific work in the GT loop (kJ/kg)
w_{CCB} : Combustion chamber blower specific work in the GT loop (kJ/kg)
$h_{C_{outlet}}$: Specific enthalpy at compressor outlet (kJ/kg)
$h_{C_{inlet}}$: Specific enthalpy at compressor inlet (kJ/kg)
$h_{CCB_{outlet}}$: Specific enthalpy at combustion chamber blower outlet (kJ/kg)
$h_{CCB_{inlet}}$: Specific enthalpy at combustion chamber blower inlet (kJ/kg)
$w_{Turbine}$: Turbine specific work in the GT loop (kJ/kg)
$h_{T_{outlet}}$: Specific enthalpy at turbine outlet (kJ/kg)
$h_{T_{inlet}}$: Specific enthalpy at turbine inlet (kJ/kg)

The heat added in the combustion chamber is computed using equation (4), while assuming air as the working fluid.

$$q_{CC} = h_{CC_{outlet}} - h_{CC_{inlet}} \quad (4)$$

With
- q_{CC} : Specific heat added in the combustion chamber (kJ/kg)
- $h_{CC_{inlet}}$: Specific enthalpy at combustion chamber inlet (kJ/kg)
- $h_{CC_{outlet}}$: Specific enthalpy at combustion chamber outlet (kJ/kg)

The system energy efficiency (η_{system}) is computed according to equation (5).

$$\eta_{system} = \frac{w_{Turbine} - w_{Compressor} - w_{CCB}}{q_{cc}} \quad (5)$$

Exergy analysis is then carried out as expressed in equation (6) in order to trace the work losses in the system, their types and quantities, in order to better inform on the possible options to reduce the inefficiencies. Energy and exergy model equations for each component are available in thermodynamic fundamentals books such as [26-28].

$$e_{in} = [w_{CV}]_{in}^{out} + \left(e_{out}^{Q} - e_{in}^{Q}\right) + e_d + e_{out} \quad (6)$$

With
- e_{in} : Specific exergy of the entering flow (kJ/kg)
- e_{out} : Specific exergy of the leaving flow (kJ/kg)
- $[w_{CV}]_{in}^{out}$: Net specific work output (kJ/kg)
- e_{out}^{Q} : Exergy of the heat rejected (kJ/kg)
- e_{in}^{Q} : Exergy of the heat added (kJ/kg)
- e_d : Exergy destruction in the system (kJ/kg)

The exergy destruction in the compressor, the CCB and the turbine are determined using equations (7) to (9), assuming no heat exchange with the surroundings.

$$e_{d_{Compressor}} = w_{Compressor} - \left(e_{C_{outlet}} - e_{C_{inlet}}\right) \quad (7)$$

$$e_{d_{CCB}} = w_{CCB} - \left(e_{CCB_{outlet}} - e_{CCB_{inlet}}\right) \quad (8)$$

$$e_{d_{Turbine}} = \left(e_{T_{inlet}} - e_{T_{outlet}}\right) - w_{Turbine} \quad (9)$$

With
- $e_{d_{Compressor}}$: Exergy destruction in the compressor (kJ/kg)
- $e_{d_{CCB}}$: Exergy destruction in the combustion chamber blower (kJ/kg)
- $e_{C_{outlet}}$: Specific exergy at compressor outlet (kJ/kg)
- $e_{C_{intlet}}$: Specific exergy at compressor inlet (kJ/kg)
- $e_{CCB_{outlet}}$: Specific exergy at blower outlet (kJ/kg)
- $e_{CCB_{inlet}}$: Specific exergy at blower inlet (kJ/kg)
- $e_{d_{Turbine}}$: Exergy destruction in the turbine (kJ/kg)
- $e_{T_{inlet}}$: Specific exergy at turbine inlet (kJ/kg)
- $e_{T_{outlet}}$: Specific exergy at turbine outlet (kJ/kg)

The heat exchanger exergy destruction is determined using equation (10):

$$e_{d_{HEX}} = \left[\left(e_{Hot_{inlet}} - e_{Hot_{outlet}}\right) + \left(e_{Cold_{inlet}} - e_{Cold_{outlet}}\right)\right] \quad (10)$$

With
- $e_{d_{HEX}}$: Exergy destruction in the heat exchanger (kJ/kg)

$e_{Hot_{inlet}}$	:	Specific exergy at the inlet of the HEX hot stream (kJ/kg)
$e_{Hot_{outlet}}$	:	Specific exergy at the outlet of the HEX hot stream (kJ/kg)
$e_{Cold_{inlet}}$	:	Specific exergy at the inlet of the HEX cold stream (kJ/kg)
$e_{Cold_{outlet}}$	:	Specific exergy at the outlet of the HEX cold stream (kJ/kg)

Finally, the exergy destruction calculations for the combustion chamber requires the use of Gibbs function value for fuel; however, it was substituted in this study by equation (11), where the average temperature in the combustion chamber is estimated from (12) [30].

$$e_{d_{CC}} = \frac{T_0}{\check{T}} . \Delta q_{CC} \tag{11}$$

$$\check{T} = \frac{\Delta q_{CC}}{\Delta s_{CC}} = \frac{h_{CC_{outlet}} - h_{CC_{inlet}}}{s_{CC_{outlet}} - s_{CC_{intlet}}} \tag{12}$$

With

$e_{d_{CC}}$	:	Exergy destruction in the combustion chamber (kJ/kg)
$\check{T}$	:	Average temperature in the combustion chamber (K)
Δq_{CC}	:	Enthalpy difference in the combustion chamber (kJ/kg)
Δs_{CC}	:	Entropy difference in the combustion chamber (kJ/kg.K)
T_0	:	Reference temperature (K)

The resulting T-S diagram of the simple Brayton cycle is illustrated in figure 3.

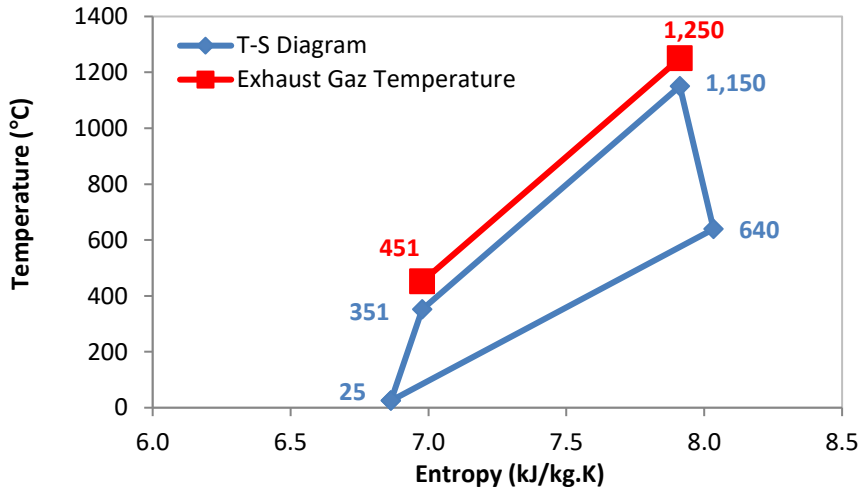

Fig. 3. T-S diagram of the external combustion gas-turbine system with maximum combustion chamber temperature of 1250°C and maximum cycle pressure of 1.2 MPa.

Exergy destruction results of the investigated simple ECGT-system are illustrated in figure 4. The figure points out the three highest shares of exergy losses, occurring in the combustion chamber (47%), in the exhaust gas released from the turbine outlet (27.7%) and in the exhaust gas from the combustion chamber outlet (15.4%).

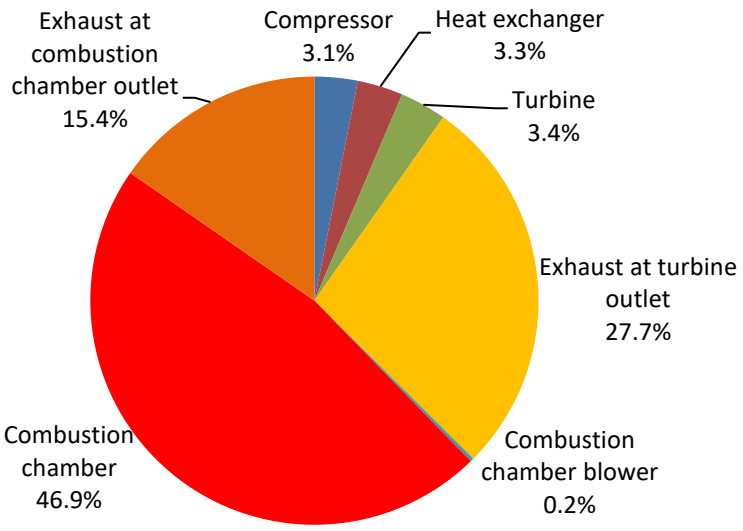

Fig. 4. Distribution of exergy destruction in the external combustion gas-turbine system with maximum combustion chamber temperature of 1250°C and maximum cycle pressure of 1.2 MPa.

It was demonstrated in several studies [30, 31] that the exergy destruction in the combustion chamber decreases as the average temperature increases. Accordingly, two ways can be considered to decrease these exergy losses: (1) increasing the combustion chamber outlet temperature while respecting metallurgic constraints, and (2) increasing the average combustion temperature through a regenerator upstream of the combustion chamber.

As for the second and third major source of exergy destruction, losses from the exhaust gases at the turbine outlet to the ambient air and from the outlet of the external combustion loop can be recovered in two ways. The first option relies on the adoption of external waste heat recovery systems or bottoming cycles (such as Rankine or Stirling among others); and the second option consists of considering internal heat recovery systems, using heat exchangers to serve as regenerators. The first option presents higher complexity for vehicle implementation since a new machine is needed, and therefore this option has been disregarded in this study.

Another important technique for exergy loss reduction at the outlet of the turbine is the adoption of a downstream shortcut, coupling the turbine outlet to the combustion chamber inlet. This technique presents on one hand the advantage of reducing the system complexity and cost since this system architecture does not require the use of a combustion chamber blower or a regenerator at the turbine outlet, and on the other hand, it avoids exergy losses in these components. Note that this solution is feasible since the only working fluid circulating in the Brayton loop is the air without any combustion products.

The exergy destruction shares of the compressor and turbine illustrated in figure 4 are negligible compared to the rest. They can be further reduced by improving the efficiency of these components.

Based on these findings, the different ECGT-system options showing a significant potential for exergy loss reduction compared to the simple ECGT system are shortlisted in table 1. These systems are classified according to the combination of the suggested techniques for exergy loss reduction such as the use of intercooling compression, reheat expansion and regenerators, as well as the downstream connection between the turbine outlet and the combustion chamber inlet, as illustrated in figure 5. The corresponding system architecture of these ECGT-systems are illustrated in figure 6, and they are considered in the rest of the study for further assessment in order to determine the most suitable ECGT-system option for an EREV application.

Table 1. Shortlisting and classification of the different ECGT-system options considered in the study.

Category		Simple ECGT	ECGT with regenerator	ECGT with downstream connection
I	Simple-compression and simple-expansion	S-ECGT	R-ECGT-1 R-ECGT-2	DS-ECGT
II	Intercooled-compression and simple-expansion	I-ECGT	IR-ECGT-1 IR-ECGT-2	DI-ECGT
III	Intercooled-compression and reheat-expansion	IRe-ECGT	IRRe-ECGT-1 IRRe-ECGT-2	DIRe-ECGT

With:

S-ECGT	:	Simple ECGT
R-ECGT-1	:	Regenerative ECGT – configuration 1
R-ECGT-2	:	Regenerative ECGT – configuration 2
DS-ECGT	:	Downstream simple ECGT
I-ECGT	:	Intercooled ECGT
IR-ECGT-1	:	Intercooled regenerative ECGT – configuration 1
IR-ECGT-2	:	Intercooled regenerative ECGT – configuration 2
DI-ECGT	:	Downstream intercooled ECGT
IRe-ECGT	:	Intercooled reheat ECGT
IRRe-ECGT-1	:	Intercooled regenerative reheat ECGT – configuration 1
IRReECGT-2	:	Intercooled regenerative reheat ECGT – configuration 2
DIRe-ECGT	:	Downstream intercooled reheat ECGT

It is important to note that assuming isothermal compression and expansion can further improve the efficiency and power density of the ECGT-systems. In fact, the isothermal compression maximizes the power density and the heat recovery process in the regenerator, and the isothermal expansion maximizes the expansion work [33, 34]. To this end, isothermal compressions and isothermal expansion are considered in the following two ECGT systems, illustrated in figures 6 (m) and (n):

- Downstream isothermal compression reheat ECGT (DIcRe-ECGT)
- Downstream isothermal compression isothermal expansion ECGT (DIcIe-ECGT)

Although isothermal processes are technically difficult to achieve and remain currently theoretical, they are considered in this study for comparison purposes, and to emphasize their additional benefits.

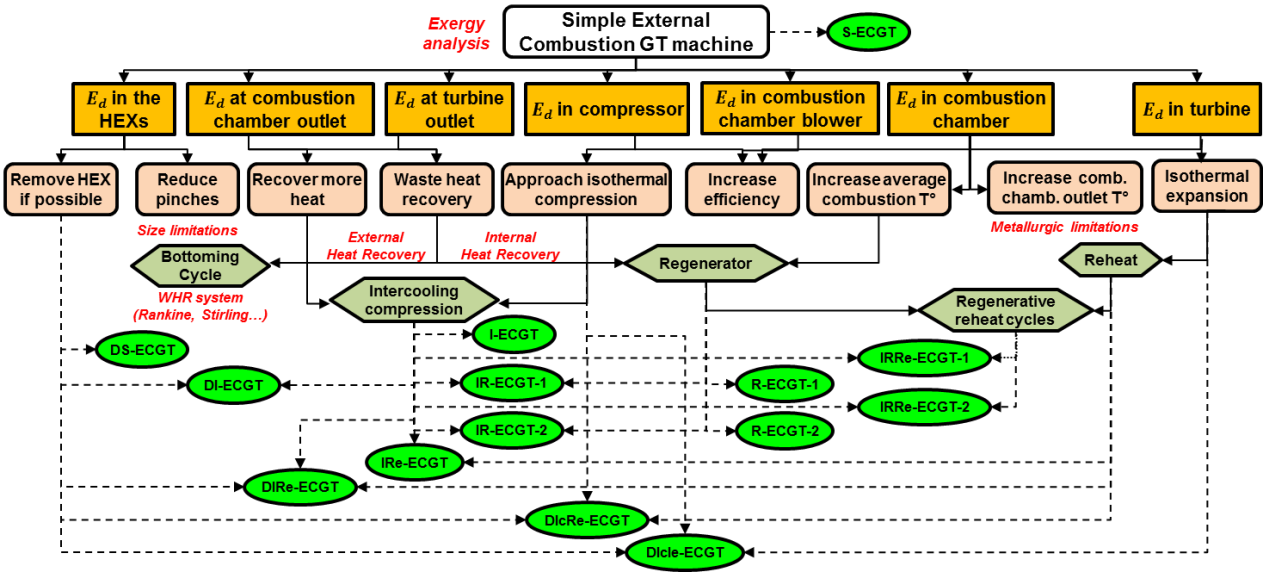

Fig. 5. Exergy assessment methodology for the identification of the ECGT-system options with reduced exergy losses.

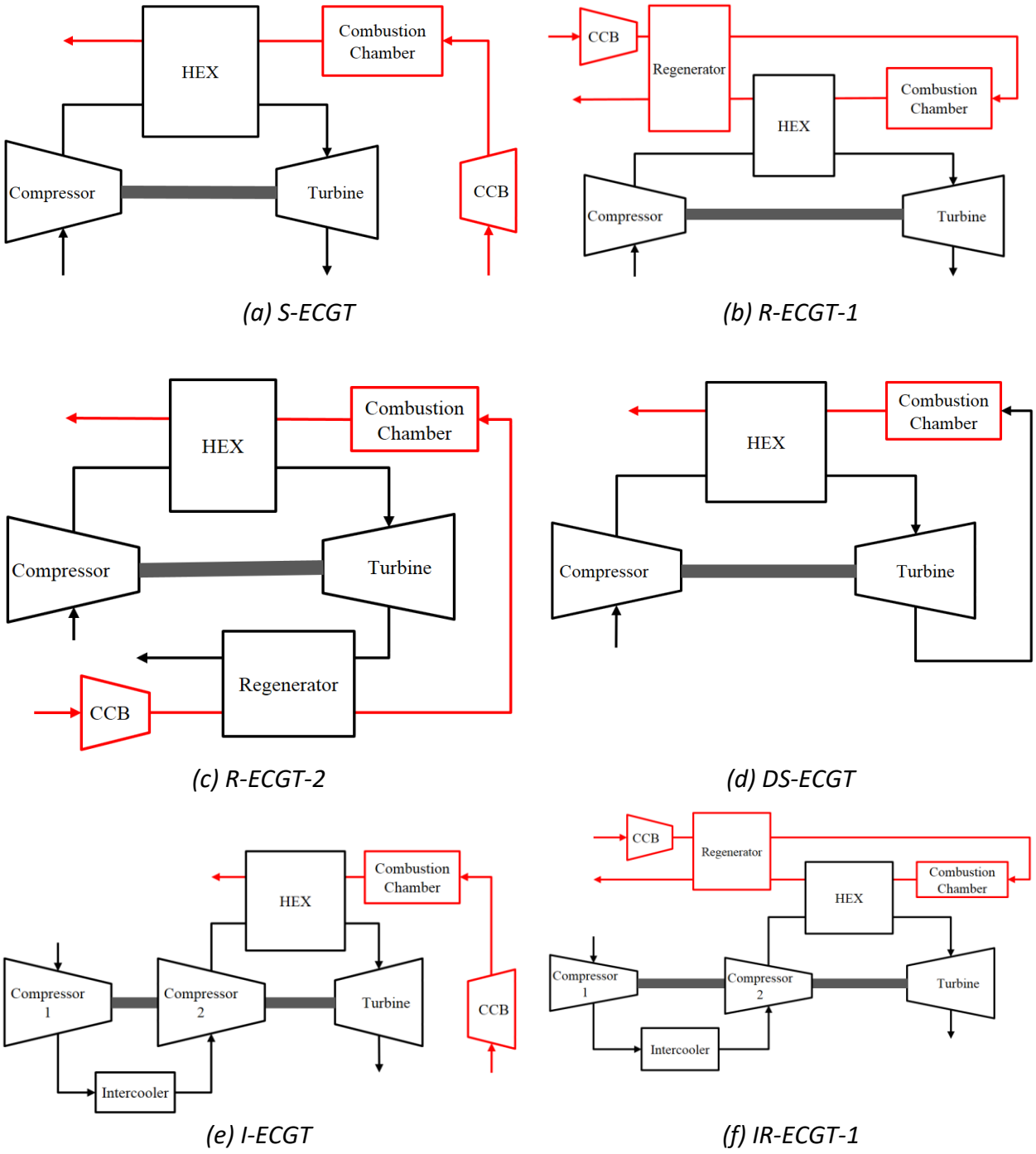

(a) S-ECGT

(b) R-ECGT-1

(c) R-ECGT-2

(d) DS-ECGT

(e) I-ECGT

(f) IR-ECGT-1

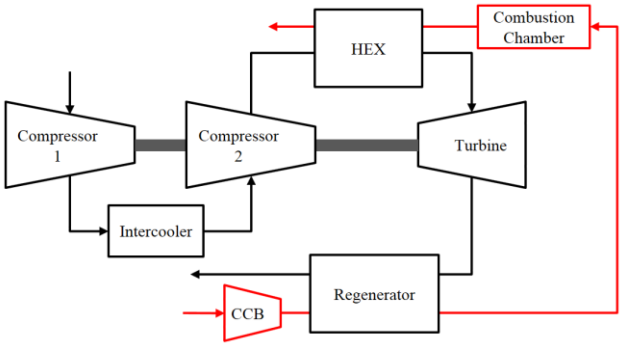

(g) IR-ECGT-2

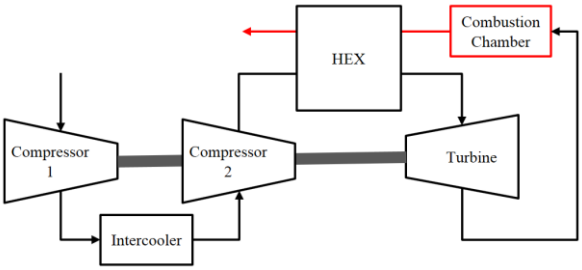

(h) DI-ECGT

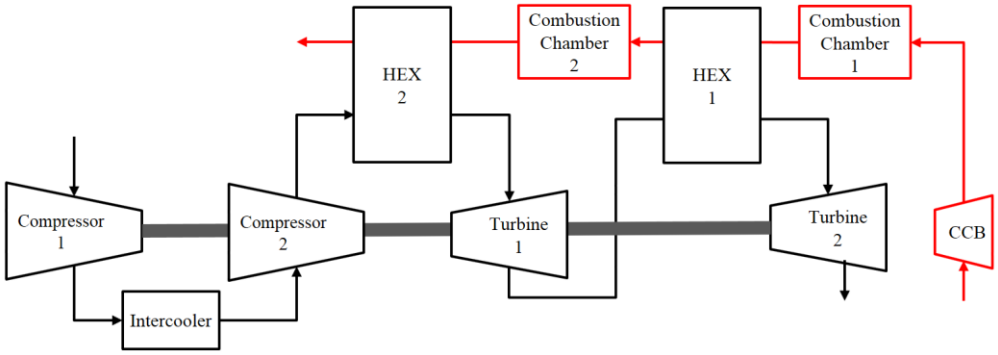

(i) IRe-ECGT

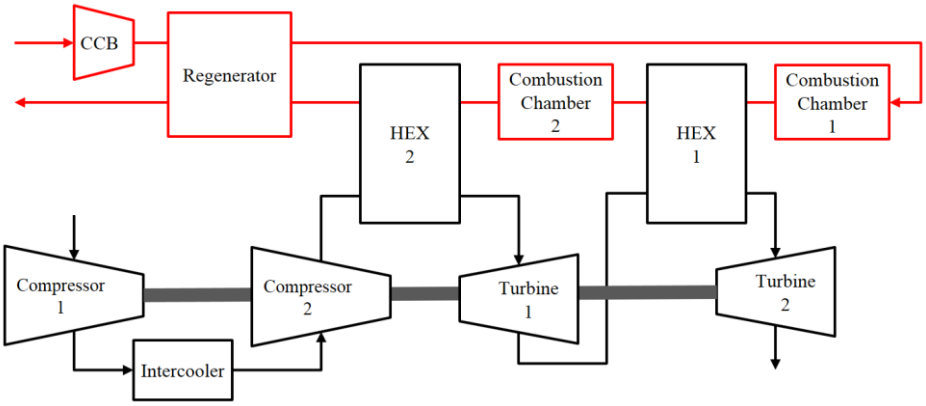

(j) IRRe-ECGT-1

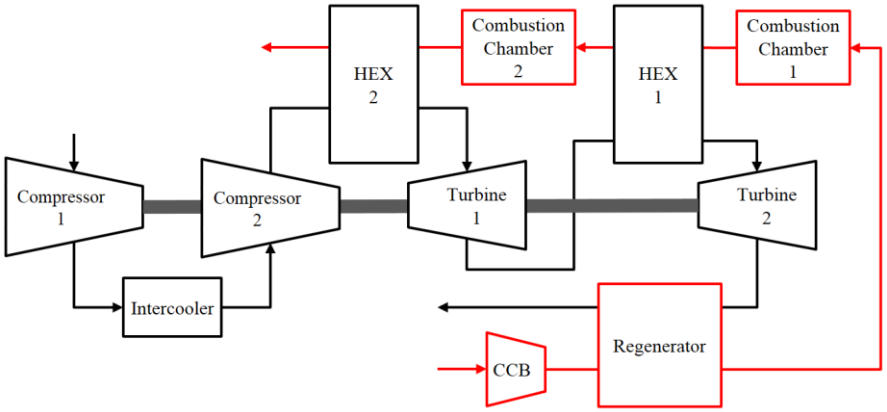

(k) IRRe-ECGT-2

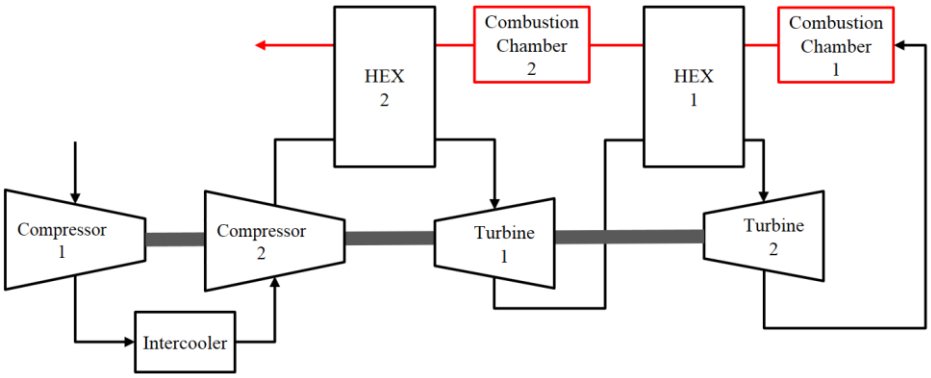

(l) DIRe-ECGT

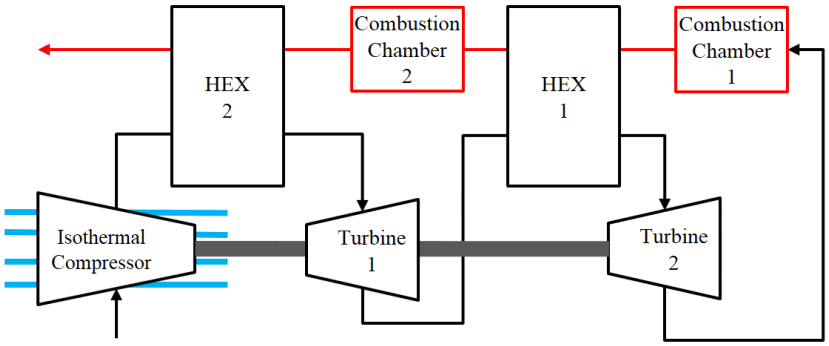

(m) DIcRe-ECGT

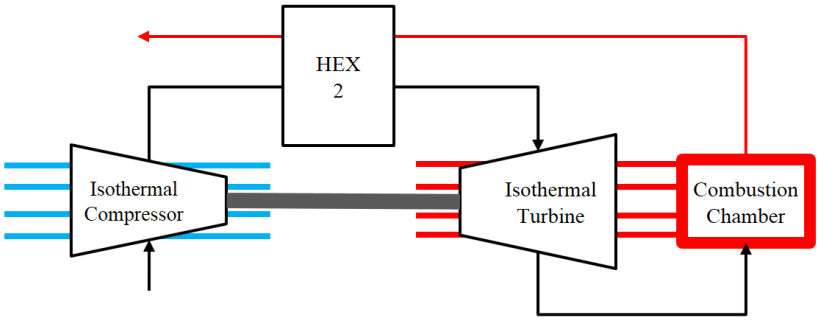

(n) DIcIe-ECGT

Fig. 6. Configuration of the different ECGT-systems considered in the analysis.

2.2. Energy and exergy analysis of identified potential gas-turbine systems

The identified ECGT-system options of figure 6 are assessed here in order to prioritize these options based on their respective efficiency and net specific work, and select the most suitable configuration. The assessment methodology for each option was presented in figure 2. The Refprop software [18] is used first to determine the thermodynamic properties of the cycle, serving to compute the energy and exergy losses in each system. Refprop uses the set of physical parameters such as the heat exchanger maximum temperature, the cycle pressure, the components efficiencies, among others; as summarized in table 2 [21, 35-39]. These parameters correspond to the state-of-the-art specifications and limitations of ECGT component technologies and to automotive design constraints.

The energy and exergy calculations are made as function of two parametric design criteria: the compression ratio (π_i) and the expansion ratio (β_j), with *i* and *j* referring to the number of compressors and turbines respectively. Therefore, the second calculation step uses the non-dominated sorting genetic algorithm (NSGA), which is a multi-objective genetic algorithm, to determine the Pareto optimal efficiency and net specific work solutions for the optimal (π_i) and (β_j) [40].

Table 2. Simulation parameters based on state-of-the-art component specifications and automotive design constraints.

Parameter	Unit	Value	Parameter	Unit	Value
Compressor technology	-	Radial	Regenerator efficiency	%	85
Max number of compression stages	-	2	Regenerator pressure drop cold side	%	4
Compressor maximum pressure ratio	-	4	Regenerator pressure drop hot side	%	3
Compressors efficiency	%	80	Combustion chamber pressure drop	%	4
Compressor inlet pressure drop	%	0.5	Max number of expansion stages	-	2
Maximum cycle pressure	MPa	1.2	Combustion chamber max T°	°C	1250
Intercoolers pressure drop	%	5	Turbines isentropic efficiency	%	85
Intercoolers outlet temperature	°C	60	Turbine expansion ratio	-	4
HEX pinches	°C	100			

Figure 7 presents the exergy losses for 1 kW of net mechanical power produced from the different considered ECGT-systems, operating at optimal efficiency. The results are grouped into three categories, according to the compression and expansion system architecture, as summarized in table 1.

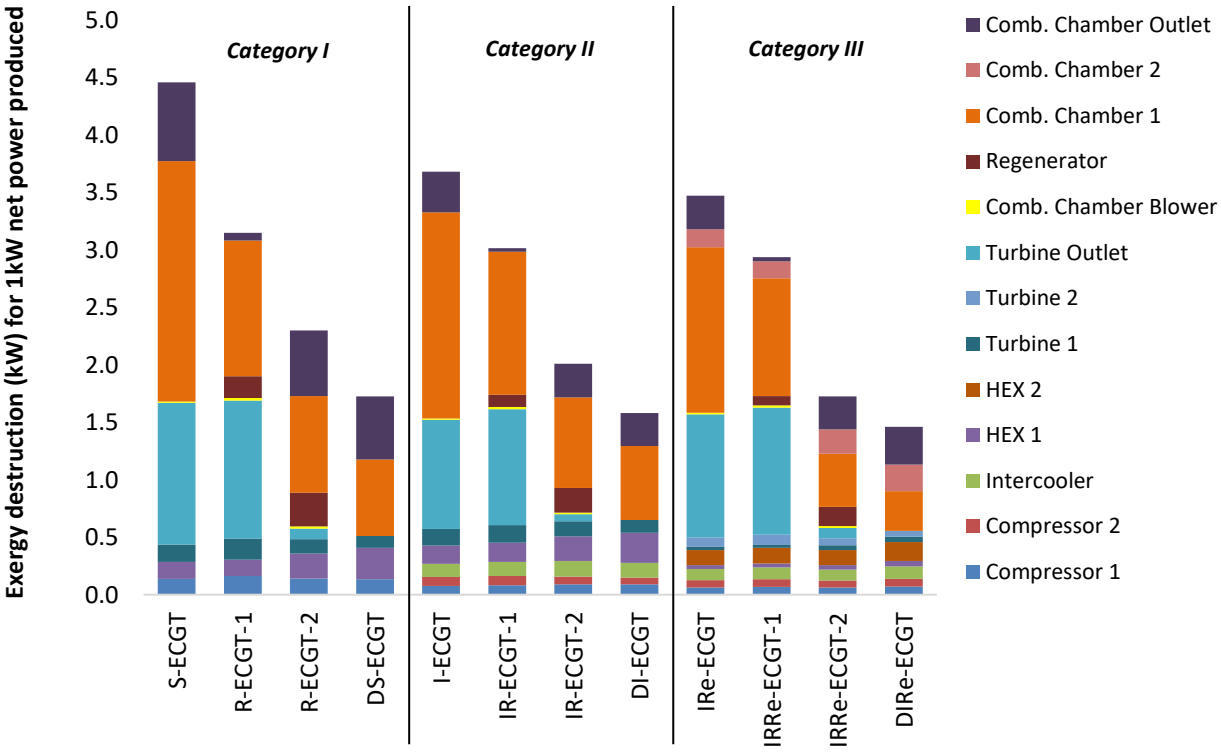

Fig. 7. Exergy destruction for 1 kW net power delivered from the different ECGT-systems.

The results of category I ECGT-systems, with simple compression and expansion, confirm the results of figure 4, where the main exergy destructions of the S-ECGT (figure 6 (a)) are in the combustion chamber, at the turbine outlet and at the outlet of the combustion chamber. Therefore, the R-ECGT-1 and R-ECGT-2 configurations consider adding a regenerator heat exchanger on the upstream of the

combustion chamber in order to increase the combustion chamber inlet temperature and reduce the combustion chamber exergy destruction as compared to the S-ECGT, since the average combustion chamber temperature has increased. However, recovering heat at the turbine outlet in R-ECGT-2 presents 29% of exergy loss reduction in the combustion chamber and 27% total exergy loss reduction compared to R-ECGT-1, which recovers heat from the combustion chamber exhaust, as illustrated in figures 6 (b) and (c). This is due to the higher turbine outlet temperature compared to the heat exchanger outlet temperature on the downstream of the combustion chamber.

The most effective system configuration in category I for exergy loss reduction is the DS-ECGT (figures 6 (d)), using a downstream shortcut to connect the turbine outlet to the combustion chamber inlet, with 61% of total exergy loss reduction compared to the S-ECGT and 25% compared to R-ECGT-2. This configuration remains the most effective to increase the combustion chamber inlet temperature without inducing heat exchanger exergy destruction penalty. It also implies a low complexity system with less components compared to R-ECGT configurations, since it eliminates the need of a regenerator and a combustion chamber blower.

Note that the same result discussions are also applicable when comparing between systems within categories II (figures 6 (e) to (h)) and III (figures 6 (i) to (l)), where the use of a downstream connection between the turbine and the combustion chamber is the most effective configuration, followed by the configuration using a regenerator recovering heat on the outlet of the turbine.

Comparing between ECGT-systems of categories I and II, the simple-compression processes in all systems of the first category (figures 6 (a) to (d)) are substituted by an intercooled-compression (figures 6 (e) to (h)). As a result, additional exergy losses reduction up to 17.4% is observed in the systems of the second category as compared to their corresponding systems of the first category. These reductions mainly occur in the combustion chamber outlet since more heat has been recovered in the heat exchanger and in the combustion chamber since less mass flow rate is required for the same output power due to the increase of the power density of these intercooled systems.

Exergy destruction results of category III systems (figures 6 (i) to (l)) shows up to 14% reduction of the total exergy losses as compared to their corresponding intercooled systems of category II and up to 25% as compared to systems of category I, despite the fact of adding a second combustion chamber and the induced additional exergy losses in this chamber. In fact, the use of a reheat system before expanding the air in the second turbine leads to higher power density, and therefore, reduces the mass flow rate and the amount of the exergy destruction in these systems.

Note that the compressors and turbines present low exergy losses compared to the heat exchangers and combustion chambers. Therefore, this illustrates the importance of the proposed explicit methodology and the exergy analysis, since it emphasizes on the importance of improving the system configuration efficiency and in particular the heat exchangers efficiency, rather than improving the isentropic efficiency of the compressors and turbines.

Based on the above exergy assessment findings, the ECGT-systems showing the lowest exergy destruction per 1 kW of net power produced will present the highest efficiency. This is reflected in the Pareto curves illustrated in figure 8, where the ECGT-systems using the downstream shortcut between the turbine outlet and the combustion chamber in the theoretical cycles with isothermal compression and expansion processes (DIcRe-ECGT and DIcIe-ECGT) as well as in the three categories (DS-ECGT, DI-ECGT and DIRe-ECGT), present the highest efficiencies among the compared systems.

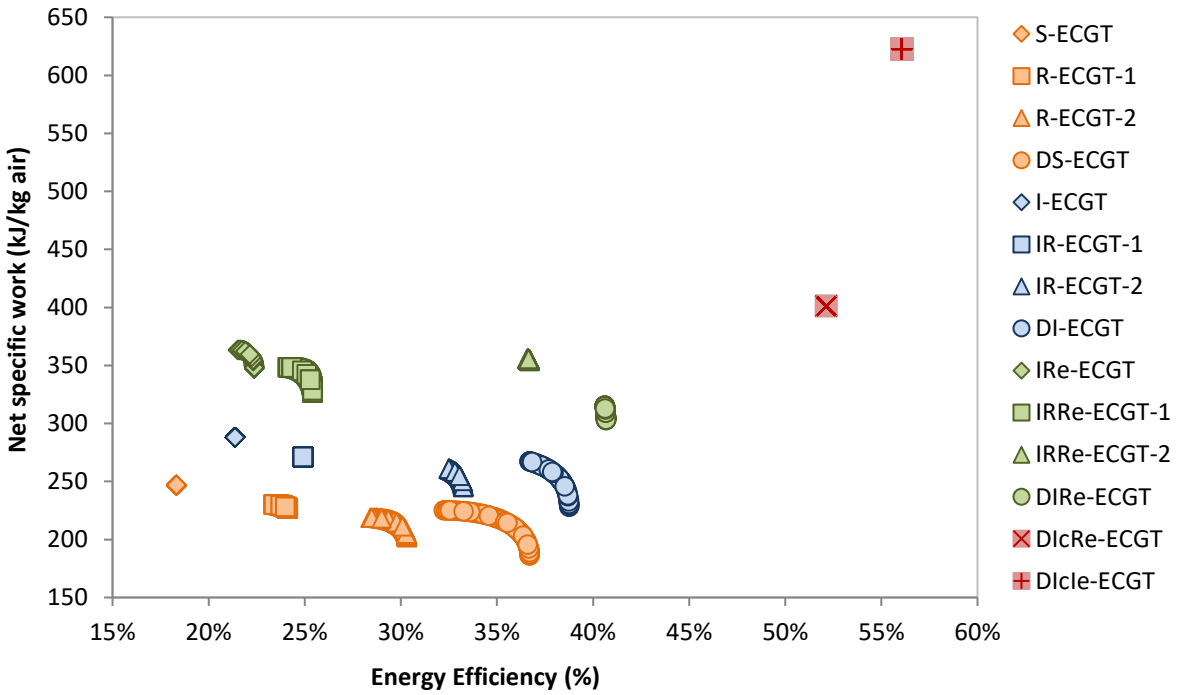

Fig. 8. Pareto optimal efficiencies and net specific work solutions of the different ECGT-systems.

Figures 9 and 10 illustrate the energy efficiency, the net specific work and the optimal compression and expansion ratio simulation results of the investigated ECGT-systems. The DIcIe-ECGT presents the highest energy efficiency and net specific work; however, as discussed in the previous section, this cycle is not realistic for implementation in EREV since it relies on isothermal compression and expansion. Consequently, DIRe-ECGT (figure 6 (l)) is the optimal-realistic ECGT-system considered for the rest of this study, which emulates the isothermal compression and expansion of the DIcIe-ECGT through a dual stage compression with an intercooler and a dual-expansion turbine with a reheat system.

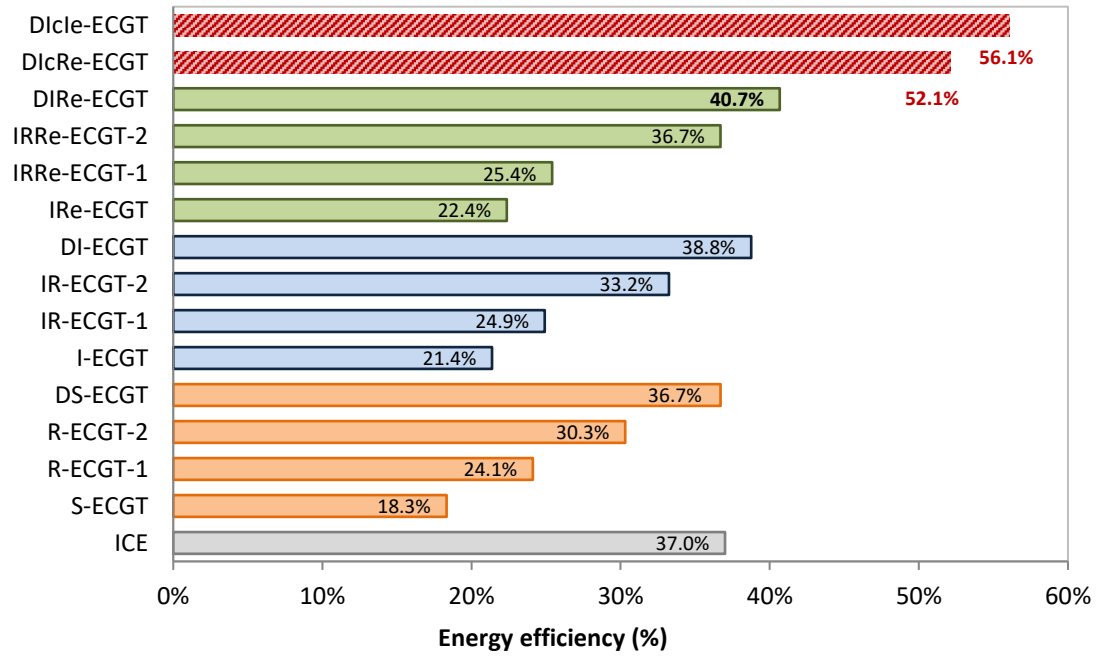

Fig. 9. Optimum energy efficiency comparison of the investigated ECGT-system options.

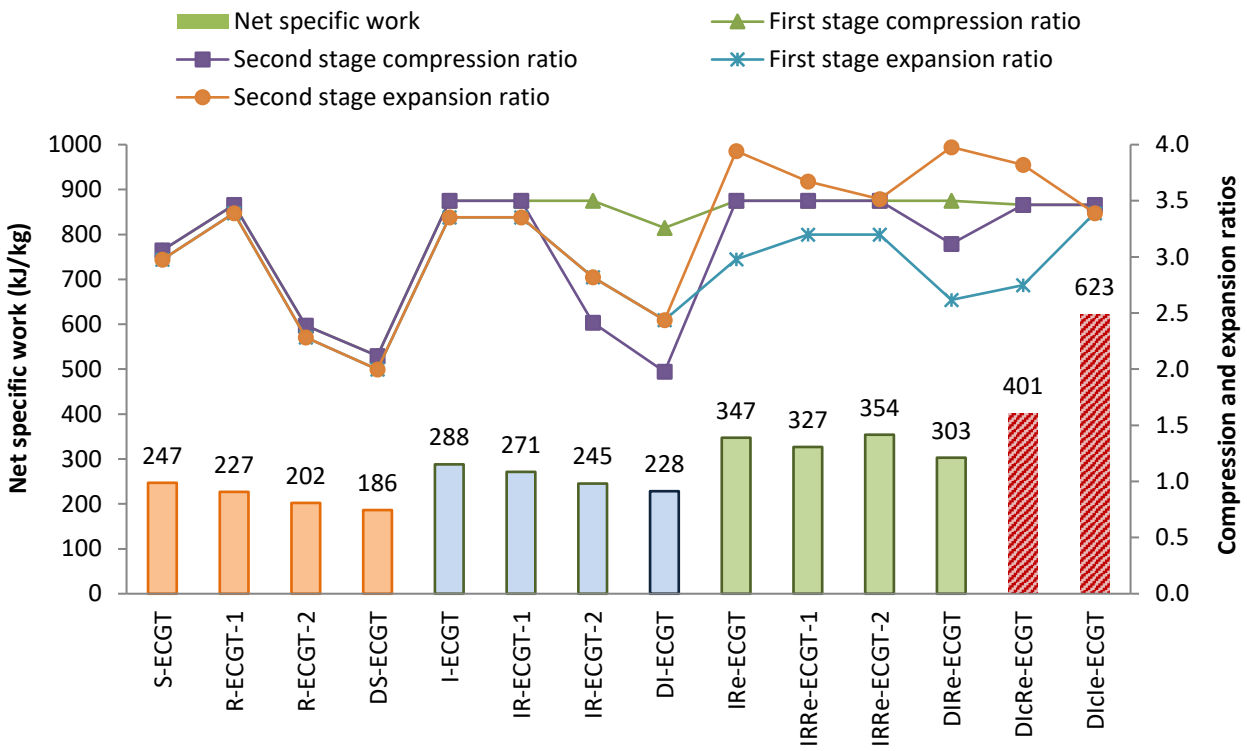

Fig. 10. Net specific work of the investigated ECGT-system options at optimal energy efficiency.

3. Vehicle Model

3.1. Powertrain setup

In order to evaluate the benefits of the DIRe-ECGT system in terms of fuel savings, a medium-class EREV with series hybrid powertrain, consisting of a DIRe-ECGT-APU and an electric traction system (as illustrated in figure 1) is modelled and presented in this section. Series hybrid powertrain configuration presents the advantage of tackling the two main deficiencies of turbine-based systems in automotive applications as discussed in the literature: the poor efficiency and the acceleration lag. On one hand, the DIRe-ECGT operates in this EREV at steady power corresponding to the optimum efficiency, which is higher than the maximum efficiency of the ICE as illustrated in figure 9. On the other hand, the vehicle is propelled by an electric motor, powered by a battery and/or the APU, and properly sized to ensure the vehicle acceleration and velocity performance without deficiency.

The vehicle parameters considered in this study are summarized in table 3. Equations (13) to (20) present the powertrain backward model, where the fuel consumption and the power flowing between the generator, the motor and the battery are determined; in addition to the battery current and the battery state of charge. The mass of the DIRe-ECGT-system, the generator and the electric motor are considered equal to the mass of the engine and its accessories. Three different battery capacities (5, 10 and 20 kWh) are considered in the analysis in order to assess the impact of the battery size on improving fuel consumption. The additional mass of the increased battery capacity is taken into account.

Table 3: Vehicle and components specifications.

Vehicle specifications	**Symbol**	**Unit**	**Value**
Vehicle mass (including driver)	M_v	kg	1210
Frontal area	S	m²	2.17
Drag coefficient	C_x	-	0.29
Wheel friction coefficient	f_r	-	0.0106
Air density	ρ	kg/m3	1.205
Wheel radius	R_w	m	0.307
Auxiliaries consumption	P_{aux}	W	750
Battery maximum power	$P_{b\,max}$	kW	50
Battery capacity	C_b	kWh	5, 10, 20
Battery mass	M_b	kg	188, 259, 356
Battery state of charge	SOC	-	[0.2, 0.4, 0.6, 0.8, 1]
Battery open circuit voltage	V_{oc}	V	[220, 224, 227, 228, 251]
Battery internal resistance	R_i	Ohm	[0.315, 0.31, 0.31, 0.335, 0.385]
IRRGT-system power	P_{GT}	kW	40
IRRGT efficiency	η_{GT}	%	46.9
Generator maximum power	P_g	kW	45
Generator maximum efficiency	η_g	%	95
Motor maximum power	P_m	kW	80
Motor maximum efficiency(1)	η_m	%	93
Transmission ratio	i	-	5.4
Transmission efficiency	η_t	%	97
Vehicle total mass	M_t	kg	$M_v + M_b$
Fuel heating value	H_v	MJ/kg	44.8
(1) The model includes a torque-speed efficiency map of the electric motor.			

$$P_{load}(t) = \left(\frac{1}{2}\rho S C_x v(t)^2 + M_t g f_r\big(v(t)\big) + M_t \frac{dv(t)}{dt}\right) \times v(t) \qquad (13)$$

$$P_m(t) = \begin{cases} \dfrac{P_{load}(t)}{\eta_t \times \eta_m}, & \dfrac{dv}{dt} \geq 0 \\ P_{load}(t) \times \eta_t \times \eta_m, & \dfrac{dv}{dt} < 0 \end{cases} \quad (14)$$

$$P_g(t) = u(t) \times P_{GT} \times \eta_g \quad (15)$$

$$P_{total}(t) = P_m(t) + P_{aux}(t) \quad (16)$$

$$P_b(t) = P_{total}(t) - P_g(t) \quad (17)$$

$$I_b(t) = \frac{V_{oc}\big(SOC(t)\big) - \sqrt{V_{oc}^2\big(SOC(t)\big) - 4P_b(t)R_i\big(SOC(t)\big)}}{2R_i\big(SOC(t)\big)} \quad (18)$$

$$SOC(t) = SOC_i(t) + \frac{1}{C_b}\int_{t_0}^{t} I_b(t)dt \quad (19)$$

$$\dot{m}_f(t) = \begin{cases} \dfrac{P_{GT}(t)}{\eta_{GT} \times H_v}, & APU{:}\,ON \\ 0, & APU{:}\,OFF \end{cases} \quad (20)$$

3.2. Energy Management Strategy

Two distinct controllers are considered in the model as illustrated in figure 1: the vehicle controller and the APU controller. The vehicle controller is responsible for delivering the driver's performance request. Hence, its main objective is to control the electric motor power in order to meet the traction and brake energy recovery demand, as presented in equation (14). The APU controller monitors the battery state of charge (SOC); thus, it controls the APU operations in order to maintain the SOC in the desired range. Therefore, an engine on/off variable $u(t)$ is considered in equation (15) in order to control the APU start operations. $u(t)$ takes the value of 0 for APU-off and 1 for APU-on.

Dynamic programming (DP) is considered in this study in order to provide the global optimal strategy to control the APU operations. The full mathematical model is presented by the authors in [24, 25]. The DP algorithm decides on the optimal strategy $U_{opt} = \{u(1), \dots, u(N)\}_{opt}$ for the scheduled route at each instant t while minimizing the fuel cost function J presented in equation (21). Consequently, DP computes backward in time from the final desired battery state of charge SOC_f to the initial state SOC_i the optimal fuel mass flow rate $\dot{m}_f\big(SOC(t), u(t)\big)$ in the discretized state time space as per equations (22) to (24). The generic DP function presented in [35] is considered in this study, with the battery SOC as state variable $x(t)$ and the APU start operations as control variable $u(t)$.

Note that the resulting optimal APU on/off strategy U_{opt} must not cause the components to violate their relevant physical boundary constraints in terms of speed, power or battery state of charge (SOC), in order to ensure their proper functioning within the normal operation range. These constraints are included in the DP model and summarized in equations (25) to (32). It is also noteworthy to mention that using DP as APU energy management strategy excludes the impact on the consumption of rule-based energy management strategies currently used on hybrid vehicles. Consequently, the obtained fuel consumption results with DP are only dependant on the investigated energy converter and its efficiency.

$$J = min\left\{\sum_{t=1}^{N} \dot{m}_f\big(SOC(t), u(t)\big) \times dt_s\right\} \quad (21)$$

with

discrete step time:	$dt_s = 1$	(22)
number of time instances:	$N = \frac{n}{dt_s}$ (with *n* the time length of the driving cycle)	(23)
state variable equation:	$SOC(t+1) = f\big(SOC(t), u(t)\big) + SOC(1)$	(24)
initial SOC:	$SOC(1) = SOC_i$	(25)
final SOC:	$SOC(N) = SOC_f$	(26)
SOC constraint:	$SOC(t) \in [0.2, 0.9]$	(27)
battery power constraint:	$P_{b_{min}} \leq P_b(t) \leq P_{b_{max}}$	(28)
motor torque constraint:	$P_{m_{min}}\big(\omega_m(t)\big) \leq P_m(t) \leq P_{m_{max}}\big(\omega_m(t)\big)$	(29)
motor speed constraint	$0 \leq \omega_m(t) \leq \omega_{m_{max}}(t)$	(30)
generator power constraint:	$P_{g_{min}}\big(\omega_m(t)\big) \leq P_g(t) \leq P_{g_{max}}\big(\omega_m(t)\big)$	(31)
generator speed constraint:	$0 \leq \omega_g(t) \leq \omega_{g_{max}}(t)$	(32)

As the optimal mass flow rate $\dot{m}_f\big(SOC(t), u(t)\big)$ is computed for the given driving cycle, the battery electric energy consumption and the powertrain efficiency are deduced using equations (33) and (34), where d is the driving cycle length, $E_{b_{traction}}$ the battery electric energy consumption to overcome the vehicle traction load, E_{ber} the vehicle load energy recovered through regenerative braking, E_{fuel} the energy of the consumed fuel and E_{grid} the consumed electric energy from the grid to recharge the battery from 30% to 80% SOC.

$$\frac{E_{b_{traction}}}{d} = \frac{1}{d}\left(E_{ber} \times \eta_m + E_{fuel} \times \eta_{APU} + E_{grid} \times \eta_{charging}\right) \quad (33)$$

$$\eta_{powertrain} = \frac{E_{traction\ load}}{E_{ber} + E_{fuel} + E_{grid}} \quad (34)$$

4. Results and discussion

Two different EREV configurations are compared in this section: the suggested DIRe-ECGT-APU and a reference ICE-APU. The DIRe-ECGT-APU is designed to operate at its optimal operating point and delivers 40 kW of mechanical power. This 40 kW power value has been adequately derived based on vehicle performance constraint. In fact, the EREV model is requested to maintain a continuous maximum velocity of 160 km/h, therefore requiring a 40 kW APU power.

The ICE-APU uses a 1.2 liters spark ignition engine with maximum efficiency of 37%. During APU operations, the ICE is allowed to operate at any point of its torque-speed map. For both models, gasoline is the fuel used, and the simulations are performed on a sequence of one to five-repeated WLTC (23 km each), covering driving distances up to 115 km. Battery initial and final SOC are 80% and 30% respectively. 5, 10 and 20 kWh battery capacities are considered.

Figure 11 illustrates the fuel and battery electric consumption trade-off on one to five-repeated WLTC. Two conclusions can be drawn from this figure:

Comparing between the different battery capacities for a given EREV model, it is obvious that the vehicle with the larger battery capacity presents the least dependence on fuel. For instance, the 20 kWh battery ICE-APU EREV consumes 32.5% less fuel than the same model with 10 kWh battery. This can also be analytically explained using equation 23, where for a given driving cycle length d, $E_{b_{traction}}$ and E_{ber} remain constant, thus increasing the battery capacity induces higher charging energy from the grid (E_{grid}) and lower fuel consumption (E_{fuel}). This comes at the expense of an increased electric drive share and therefore, would displace the emissions to the power plants if these EREVs are recharged with dirty electricity, and their overall contribution to the mitigation of global warming and improving air quality in cities is reduced.

Comparing between the two EREV models for a given battery capacity, the ICE-APU EREV shows additional fuel consumption as compared to the DIRe-ECGT-APU EREV. For instance, the latter with a 20 kWh battery consumes over five-repeated WLTC 9.7% less fuel as compared to the similar ICE-APU EREV model. This is entirely due to the improved efficiency of the APU system as both models consumed the same battery electric energy by the end of the trip. Figure 12 shows 51.8% and 56.4% powertrain efficiency of the ICE-APU EREV and the DIRe-ECGT-APU EREV models respectively, for this specific example. This can be analytically demonstrated from equation 23, where assuming the same driving cycle length d, and for a given battery capacity, $E_{b_{traction}}$, E_{ber} and E_{grid} are the same for both models; consequently, improving the APU efficiency induces a decrease in fuel consumption.

The powertrain efficiency curves illustrated in figure 12 are derived using equation (34). It is noteworthy to mention that for short driving cycle length d (1 WLTC) and large battery capacities (10 and 20 kWh), the APU is not required to turn on, and the whole distance is travelled in electric mode only. Thus, the electric consumption of both models converges to 211 Wh/km for the 10 kWh battery and 218 Wh/km for the 20 kWh, as illustrated in figure 11. The additional consumption of the 20 kWh battery is due to the additional carried weight of the battery.

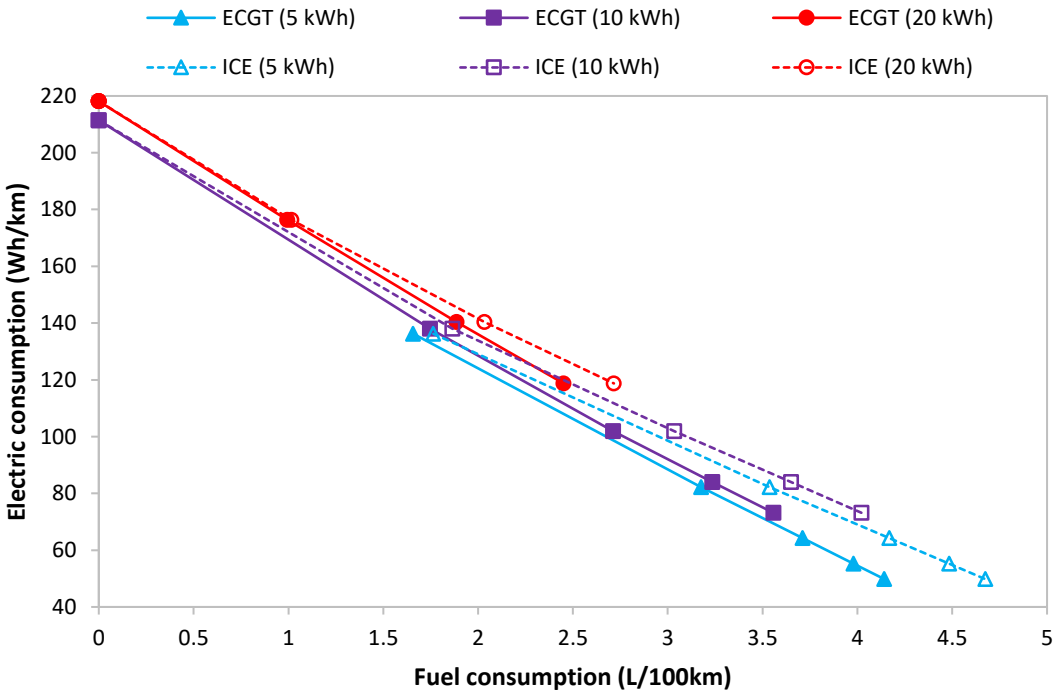

Fig. 11. Electric and fuel consumption trade-off on one to five-repeated WLTC.

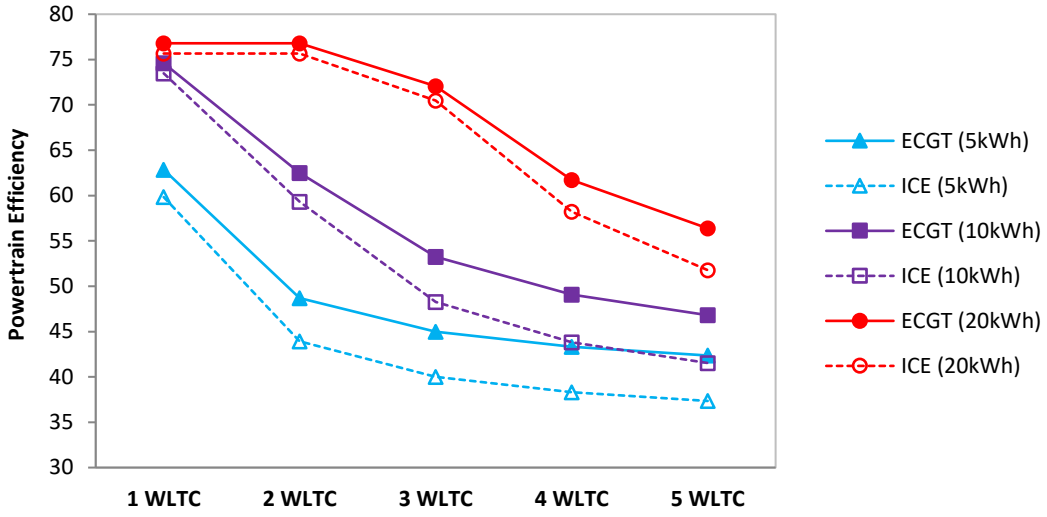

Fig. 12. Powertrain efficiency on one to five-repeated WLTC.

Comparing the fuel consumption results between the DIRe-ECGT-APU and the ICE-APU in figure 13, 6% to 11.5% fuel savings are observed. As detailed above, these savings are explained by the higher operating efficiency of the DIRe-ECGT since it was constrained to operate at its optimal efficiency of around 40.7%. Although the ICE was not constrained to operate at one operating point, results showed that ICE operation was at the optimal operating line where the efficiency remains between 36 and 37%, almost at its maximum efficiency of 37%.

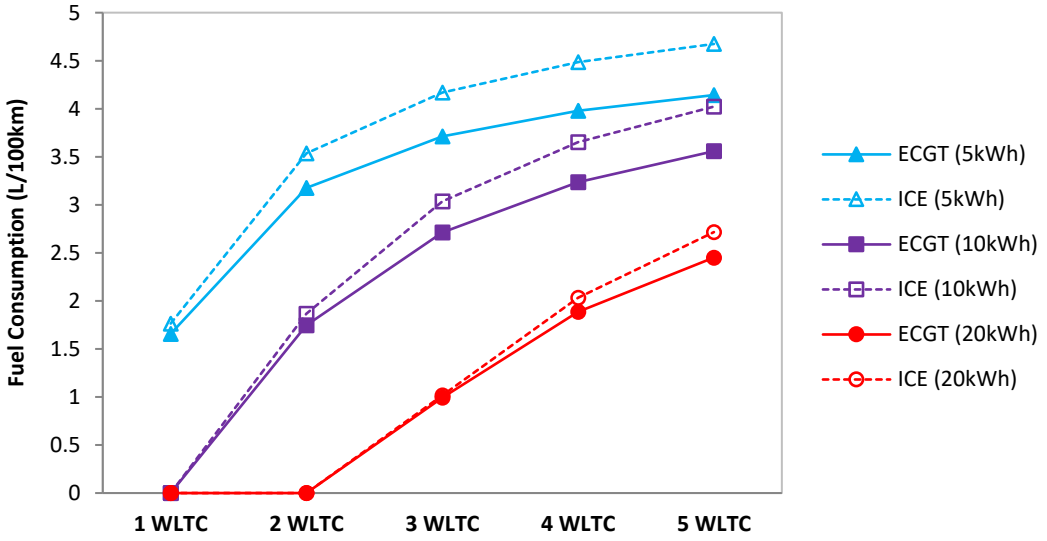

Fig. 13. Fuel consumption of the DIRe-ECGT and ICE EREV models on one to five-repeated WLTC.

5. Conclusion

An energy and exergy analysis as well as components and automotive technological constraints are applied in this study to identify the suitable Brayton external combustion gas-turbine (ECGT) system for extended range electric vehicles (EREV). The Downstream intercooled reheat ECGT (DIRe-ECGT) was selected. It offered the highest efficiency among the several ECGT-system options and conventional internal combustion engines (ICE). An EREV with a series hybrid powertrain is modeled and the DIRe-ECGT and ICE auxiliary power units (APU) are simulated and compared in terms of fuel consumption using the dynamic programming optimal control as APU management

strategy. A parametric study was also conducted in order to evaluate the impact of battery capacity and mass on fuel consumption.

Simulation results showed that the DIRe-ECGT-system offers 6% to 11.5% fuel consumption savings compared to similar ICE configuration. Results also highlighted the interest of considering large battery capacities for maximizing fuel savings. 66.5% and 32.5% of fuel savings were observed on one and five-repeated WLTC respectively between 20 kWh and 10 kWh battery models. However, this advantage came at the expense of an increased vehicle cost and battery volume, which was not discussed in this study.

The methodology presented in this study will be further elaborated in order to evaluate the fuel consumption saving for ECGT-systems on different vehicle applications ranging from small to large and sport utility extended range electric vehicles. Simulations will include real driving cycles and other vehicle energetic criteria such as the cabin thermal needs.

References

[1] Cracknell, R., Kramer, G., and Vos, E., "Designing Fuels Compatible with Reformers and Internal Combustion Engines," SAE Technical Paper 2004-01-1926, 2004, https://doi.org/10.4271/2004-01-1926.

[2] Martin Kautz and Ulf Hansen, “The Externally Fired Gas Turbine (EFGT-Cycle) for decentralized use of biomass”, Applied Energy, Volume 84, Issues 7-8, July-August 2007

[3] L. Eidensten, J. Yan and G. Svedberg, “Biomass Externally Fired Gas Turbine Cogeneration” *J. Eng. Gas Turbines Power* 118(3), 604-609 (Jul 01, 1996), doi:10.1115/1.2816691

[4] Guoquan Qiu, Hao Liu, Saffa Riffat, “Expanders for micro-CHP systems with organic Rankine cycle”, Applied Thermal Engineering, Volume 31, Issue 16, November 2011, https://doi.org/10.1016/j.applthermaleng.2011.06.008

[5] Amir A. Aliabadi, Murray J. Thomson*, James S. Wallace, Tommy Tzanetakis, Warren Lamont and Joseph Di Carlo, “Efficiency and Emissions Measurement of a Stirling-Engine-Based Residential Microcogeneration System Run on Diesel and Biodiesel”, *Energy Fuels*, 2009, 23 (2), pp 1032–1039, DOI: 10.1021/ef800778g

[6] Carlos Ulloa, Jacobo Porteiro, Pablo Eguia and José M. Pousada-Carballo, “Application Model for a Stirling Engine Micro-Generation System in Caravans in Different European Locations”, Energies 2013, 6, 717-732; doi: 10.3390/en6020717

[7] S. Bonnet, M. Alaphilippe and P. Stouffs, « Energy, exergy and cost analysis of a micro-cogeneration system based on an Ericsson engine », International Journal of Thermal Sciences, https://doi.org/10.1016/j.ijthermalsci.2005.09.005

[8] M. Petach, E. Tward, and S. Backhaus, “Design of a High Efficiency Power Source (HEPS) Based on Thermoacoustic Technology,” Final report, NASA contract no. NAS3-01103, CDRL 3f, 2004

[9] K. Qiu and A.C.S. Hayden, “Integrated thermoelectric and organic Rankine cycles for micro-CHP systems”, Applied Energy, September 2012, https://doi.org/10.1016/j.apenergy.2011.12.072

[10] William C. Strack, “Condensers and Boilers for Steam-Powered Cars: A Parametric Analysis of their Size, Weight, and Required Fan Power”, NASA Technical note, NASA TN D-5813

[11] Rosenqvist, K., Lia, T., and Goldwater, B., "The Stirling Engine for the Automotive Application," SAE Technical Paper 790329, 1979, https://doi.org/10.4271/790329

[12] History of Chrysler Corporation Gas Turbine Vehicles, Chrysler Corporation, January 1979.

[13] Sandro B. Ferreira and Pericles Pilidis, “Comparison of Externally Fired and Internal Combustion Gas Turbines Using Biomass Fuel”, *J. Energy Resour. Technol* 123(4), 291-296, 2001, doi:10.1115/1.1413468

[14] Alberto Traverso, Aristide F. MAssardo and Riccardo Scarpellini, “Externally Fired micro-gas turbine: Modelling and expeimental performance”, Applied Thermal Engineering, Volume 26, Issue 16, November 2006, https://doi.org/10.1016/j.applthermaleng.2006.01.013
[15] Magali Roquette, Sandro Barros Ferreira, Anthony J.B. Jackson and Pericles Pilidis, “Performance and Optimisation of Externally Fired Gas Turbines Fuelled with Biomass”, Proceedings of COBEM 2005, the 18th International Congress of Mechanical Engineering, November 6-11, 2005, Ouro Preto, MG.
[16] Leonardo Pierobon, tuong-Van Nguyen, Andrea Mazzucco, Ulrik Larsen and Frederik Haglind, “Part-Load Performance of a Wet Indirectly Fired Gas Turbine Integrated with an Organic Rankine Cyce Turbogenerator”, Energies 2014, 7, 8294-8316; ISSN 1996-1073, doi:10.3390/en7128294
[17] Bou Nader, W., Mansour, C., Nemer, M. and Guezet, O., “Exergo-technological explicit methodology for gas-turbine system optimization for series hybrid electric vehicles”, Proceedings of the Institution of Mechanical Engineers, Part D: Journal of Automobile Engineering, 2017
[18] Lemmon, E. W., McLinden, M. O., & Huber, M. L. (2002). NIST Standard Reference Database 23-NIST Thermodynamic and Transport Properties REFPROP, Version 7.0 (No. World Wide Web-Internet and Web Information Systems).
[19] Saeed Soltani, Hassan Athari, Marc A. Rosen, Seyed Mohammad Seyed Mahmoudi and Tatiana Morosuk, “Thermodynamic Analyses of Biomass Gasification Integrated Externally Fired, Post-Firing and Dual-Fuel Combined Cycles”, Sustainability 2015, 7, 1248-1262; doi: 10.3390/su7021248
[20] Elmegaard, B., Qvale, E. B., Carapelli, G., & deFaveriTron, P., « Open-cycle indirectly fired gas turbine for wet biomass fuels”. In Proceedings of Efficiency, Cost, Optimization, Simulation and Environmental Impact of Energy Systems (pp. 361-367). Istanbul: International Centre for Applied Thermodynamics, 2001.
[21] J. Yan and L. Eidensten. "Status and Perspective of Externally Fired Gas Turbines", Journal of Propulsion and Power, Vol. 16, No. 4 (2000), pp. 572-576. https://doi.org/10.2514/2.5641
[22] S Bram, J De Ruyck and A Novak-Zdravkovic, “Status of external firing of biomass in gas turbines”, Proceedings of the Insitution of Mechanical Engineers, Part A: Journal of Power and Energy, 2005
[23] Sergio M. Camporeale, Antonio M. Pantaleo, and Bernardo Fortunato, “Cycle configuration analysis and techno-economic sensitivity of biomass externally fired gas turbine with bottoming ORC”, Energy Conversion and Management, Volume 105, 15 November 2015, Pages 1239-1250.
[24] Mansour C. Trip-based optimization methodology for a rule-based energy management strategy using a global optimization routine: the case of the Prius plug-in hybrid electric vehicle. In: *Proceedings of the Institution of Mechanical Engineers*. Part D: *Journal of Automobile Engineering*, Vol 230, Issue 11, pp. 1529 – 1545, 2015.
[25] Mansour C. Optimized energy management control for the Toyota Hybrid system using dynamic programming on a predicted route with short computation time. *In: International Journal of Automotive Technology*. Paper N° 220100321, vol.13, No. 2, 2012.
[26] Sonntag R and Borgnakke R. Fundamentals of Thermodynamics, Sixth Edition, 2003, p.411-423.
[27] Moran M and Shapiro H. Fundamentals of engineering thermodynamics. 5th Edition – 2006, p.303-308.
[28] J.H. HORLOCK, “Advanced Gas Turbine Cycles”, ISBN 0-08-044273-0, Pergamon, 2003
[29] S. Soltani, M. Yari, S.M.S. Mahmoudi, T. Morosuk and M.A. Rosen, “Advanced exergy analysis applied to an externally-fired combined-cycle power plant integrated with a biomass gasification unit”, Energy, Volume 59 15 September 2013, Pages 775-780

[30] Datta A and Som S. Energy and exergy balance in a gas turbine combustor. J Power Energy - Proc Inst Mech Eng, 213:23–32, 1999.

[31] W. R. Dunbar and N. Lior, “Sources of combustion irreversibility”, Combustion Science and Technology, Volume 103, 1994 – Issue 1-6.

[32] S.K. Som and A. Datta, “Thermodynamic irreversibilities and exergy balance in combustion processes”, Progress in Energy and Combustion Science, Volume 34, Issue 3, June 2008.

[33] Sirignano W and Liu F. Performance increase for gas-turbine engines through combustion inside the turbine. In: *Journal of Propulsion and Power.* Vol.15, No. 1, January - February 1999.

[34] Jubleh N. Exergy analysis and second law efficiency of a regenerative brayton cycle with isothermal Heat Addition. Entropy ISSN 1099-4300, 2005.

[35] Martin Kautz and Ulf Hansen, “The Externally Fired Gas Turbine (EFGT-Cycle) and Simulation of the Key Components”, University of Rostock, Institute for Energy and Environment Technology, Rostock, Germany.

[36] Fredrik Olsson, Sven-Ake Svensson and Roddy Duncan, “Externally Fired Gas Turbine Cycles with High Temperature Heat Exchangers Utilising Fe-based ODS Alloy Tubing”, 15th International Plansee Seminar, 2001.

[37] Baum J. “Studies regarding the externally fired gas turbine process with a high temperature heat exchanger”, Fortschitt Berichte VDI, Reihe 8. Energietechniek, 2001.

[38] Mao C., Scarpellini R., Valarani M. “Design, construction and testing of a ceramic high temperature heat exchanger for an externally fired cycle plant”. Schriften der Forschunszentrums Juelich, Energy Technol., 2002, 21, 845–852.

[39] K.A. Al-attab and Z.A. Zainal, “Performance of high-temperatureheat exchangers in biomass fuel powered externally fired gas turbine systems”, Renewable Energy, Volume 35, Issue 5, May 2010

[40] Deb K, Pratap A, Agarwal S et al. A fast and elitist multiobjective Genetic Algorithm: NSGA-II. In: *IEEE Transactions on evolutionary computation*, Vol. 6, No. 2, APRIL 2002.